

## Multimodal Deep Learning for Predicting Drug–Transporter Binding in Anxiety Disorders

Yanzhe Wang

The High School Affiliated to Renmin University of China, Beijing, China

elliotwyz@163.com

**Keywords:** Unsupervised learning; Multimodal representation; Mind-body state modeling

**Abstract:** Anxiety disorders affect over 300 million people worldwide, highlighting the urgent need for efficient drug discovery. Current treatments target neurotransmitter transporters, but traditional development is slow and costly. We propose a fully connected neural network framework that integrates molecular descriptors from small molecules (via Mordred) with structural features of transporters predicted by AlphaFold. This multimodal representation enables accurate prediction of drug-transporter binding affinity. Experiments show that our model outperforms classical machine learning baselines and that combining ligand and protein features yields the best results. The framework provides a scalable tool for screening candidate anxiolytic drugs potentially accelerating discovery and reducing trial-and-error costs.

### 1. Introduction

Anxiety and diminished self-confidence are increasingly recognized as serious threats to individual well-being and global public health. According to the World Health Organization, approximately 301 million people worldwide suffer from anxiety disorders, representing about 4% of the global population [1]. Such conditions not only impair daily functioning, but also increase risks of comorbid psychiatric illnesses and reduced quality of life.

Neurotransmitters are chemical messengers that mediate communication between neurons in the central nervous system. After being released into the synaptic cleft, neurotransmitters bind to post-synaptic receptors, and their signaling is terminated primarily by reuptake through neurotransmitter transporters [2]. These transporter proteins tightly regulate neurotransmitter concentration and duration of action. Current anxiolytic drugs often target transporter activity, either by inhibiting reuptake to increase neurotransmitter levels in the synaptic cleft or by modulating transporter function to rebalance neurotransmission. Classic examples include selective serotonin reuptake inhibitors (SSRIs) such as fluoxetine and sertraline, and serotonin-norepinephrine reuptake inhibitors (SNRIs) such as venlafaxine and duloxetine [3].

With the rapid advancement of deep learning, artificial intelligence (AI) has made groundbreaking contributions in the life sciences. In 2024, the Nobel Prize in Chemistry was awarded to the developers of AlphaFold, a deep learning model that revolutionized protein structure prediction, underscoring the transformative role of AI in computational biology [4, 5]. These breakthroughs have opened new avenues for drug discovery, particularly in understanding protein-ligand interactions.

In parallel, quantitative structure-activity relationship (QSAR) modeling has long served as a computational strategy for correlating molecular structure with biological activity [6]. Integrating deep learning with QSAR allows for large-scale screening of small molecules with predicted high affinity for biological targets, such as neurotransmitter transporters. In the context of developing anxiolytic and confidence-enhancing drugs, AI-driven approaches could greatly accelerate the identification of candidate compounds and expand therapeutic options for patients.

Previous research on transporter-targeted drug discovery has provided valuable insights, but existing methods face two major limitations: (1) insufficient generalizability, as most models are designed for individual transporters and do not generalize across protein families; and (2) over-reliance on molecular descriptors alone, neglecting essential protein features such as three

dimensional structure and physicochemical properties, which are critical for accurate affinity prediction [7].

In this study, we propose an integrated computational framework that combines molecular descriptors of small molecules with structural features of neurotransmitter transporters, as illustrated in Fig. 1. Candidate molecules were represented in SMILES format and processed using the Mordred library to extract geometric, topological, and physicochemical descriptors. [8]. Protein structures of anxiety-related neurotransmitter transporters (including serotonin and norepinephrine transporters) were predicted using AlphaFold [4]. These molecular and protein features were fused in a fully connected neural network to predict binding affinities. We divided the dataset into training (80%) and external testing (20%), applied five-fold crossvalidation on the training set, and evaluated performance using multiple predictive metrics. Our results demonstrate that incorporating protein features significantly improves predictior accuracy, offering a scalable approach for screening anxiolytic drug candidates.

The main contributions of this work can be summarized as follows:

- We propose an integrative framework that combines small-molecule descriptors with protein structural features predicted by AlphaFold, enabling a more comprehensive representation of ligand-transporter interactions.
- Unlike previous QSAR models that only consider molecular descriptors, our method explicitly incorporates the spatial and physicochemical characteristics of neurotransmitter transporters, thus improving affinity prediction accuracy and model generalization.
- We systematically evaluate our model across multiple neurotransmitter transporters related to anxiety regulation (e.g., serotonin and norepinephrine transporters), using fivefold cross-validation and external testing to ensure robustness.
- Our approach provides a scalable computational tool for accelerating anxiolytic drug discovery, offering a potential strategy to reduce the trial-and-error process and multitarget side effects in current pharmacological research

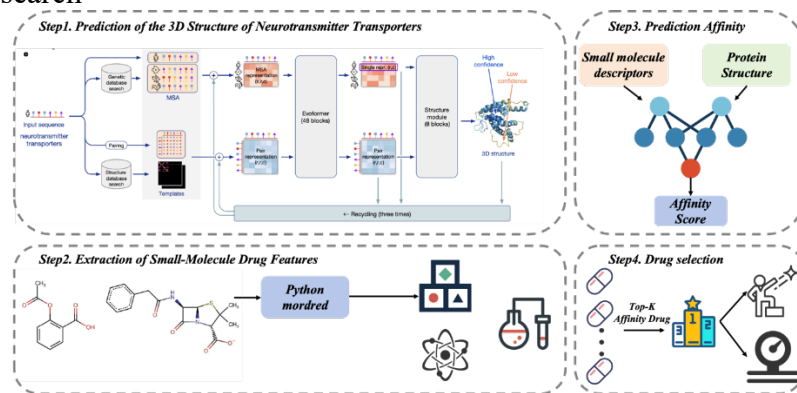


Figure 1 Overall workflow of the proposed framework for transporter-drug interaction analysis.

## 2. Dataset

### 2.1. Data sources

We compiled ligand-transporter binding data from four open resources: BindingDB ChEMBL, PubChem and ZINC [9, 10, 11,12]. We focused on human neurotransmitter transporters strongly implicated in mood and anxiety regulation, such as the serotonin transporter (SLC6A4), norepinephrine transporter (SLC6A2), dopamine transporter (SLC6A3), vesicular monoamine transporter (SLC18A2), GABA transporter (SLC6A1) and glycine transporter (SLC6A9). UniProt was used to map target identifiers and sequences [13]. Table 1 summarizes the transporters included in this study.

### 2.2. Data collection and curation

Data were retrieved programmatically via API and bulk downloads. For transporters we retained

only records that were clearly mapped to human targets (UniProt mapping) and that contained direct binding or inhibition measurements (Ki, Kd, IC50, EC50 or similar). For small molecules, canonical SMILES served as the primary representation. Additional small molecules were randomly sampled from ZINC to balance the dataset and generate negative examples [12].

All molecule structures were standardized using RDKit [14] following ChEMBL's curation guidelines [15]. Standardization included salt/solvent removal, charge normalization, and canonical SMILES generation. Records were filtered to retain only numeric affinity values and duplicate ligand-target pairs were aggregated by taking the median of converted affinities. Duplicates and stereochemical inconsistencies were removed. This curation strategy aligns with best practices recommended by ChEMBL and BindingDB.

### 2.3. Label processing

Affinity measurements were unified on a nanomolar (nM) scale. When assay parameters permitted, IC50 values were converted to estimated  $K_i$  using the Cheng-Prusoff relation [16]. Both raw affinity values and log-transformed labels ( $p\text{Affinity} = -\log_{10}(\text{Affinity in M})$ ) were stored for modeling. This dual labeling facilitated both regression and classification tasks.

### 2.4. Molecular descriptor extraction

Molecular features were extracted from canonical SMILES. Two-dimensional descriptors were derived directly from the SMILES strings, covering constitutional, topological, and fingerprint-like properties. For three-dimensional descriptors, low-energy conformers were generated using RDKit's UFF/MMFF force fields, followed by Mordred descriptor computation [17]. To ensure feature stability, descriptors with over 30 % missing values or near-zero variance were removed, and remaining missing entries were imputed with the median. Highly correlated descriptors (Pearson  $r > 0.95$ ) were filtered to reduce collinearity. Finally, features were standardized (z-score scaling) using scikit-learn. Table 1 summarizes the descriptor categories.

### 2.5. Protein structural and sequence features

Protein sequences were obtained from UniProt [13], and when experimental structures were unavailable, AlphaFold predictions were used [18]. From sequences, we extracted amino acid composition, molecular weight, isoelectric point, and other physicochemical summaries. Structural features included secondary-structure composition (via DSsP [18]), solvent-accessible surface area and residue exposure statistics (via FreeSASA [19]), radius of gyration, and contact-map summaries. Known functional motifs and transmembrane helix counts from UniProt annotations were also included. These features ensured that both sequence-level and structure-derived properties were incorporated into the model (Table 2).

Table 1 List of neurotransmitter transporters studied, with gene names and UniProt identifiers.

Transporter	Gene	UniProt ID	Main function
Serotonin transporter	SLC6A4	P31645	Uptake of serotonin (5-HT)
Norepinephrine transporter	SLC6A2	P23975	Uptake of norepinephrine
Dopamine transporter	SLC6A3	Q01959	Uptake of dopamine
Vesicular monoamine transporter 2	SLC18A2	Q05940	Storage of monoamines in vesicles
GABA transporter 1	SLC6A1	P30531	Uptake of GABA
Glycine transporter 1	SLC6A9	P48067	Uptake of glycine

Table 2: Descriptor categories extracted for ligands and transporters.

Category	Description
Molecular 2D descriptors	Constitutional, topological, fingerprint counts
Molecular 3D descriptors	Geometrical, charge-related, conformer-derived features
Protein sequence features	Amino acid composition, molecular weight, pI
Protein structural features	Secondary structure fractions, SASA, radius of gyration
Contact-map summaries	Mean/variance of pairwise residue distances
Functional annotations	Motifs, TM helices from UniProt

### 3. Methods

In this work, we designed a fully connected neural network (FCNN) to predict the binding affinity between small molecules and neurotransmitter transporters. The model integrates molecular descriptors extracted from ligands and structural features derived from protein sequences, producing a unified representation for regression-based affinity prediction, as illustrated in Fig. 2.

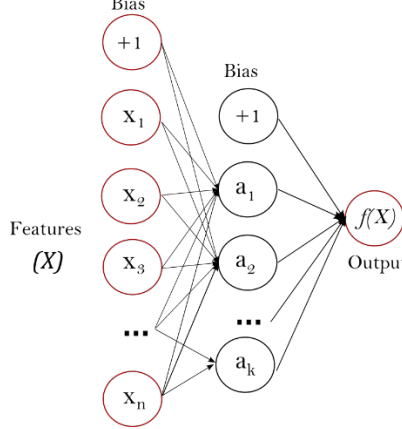


Figure 2 Schematic architecture of the fully connected neural network(FCNN).The input consists of concatenated molecular descriptors and protein structural features, which are processed by multiple hidden layers to produce a continuous affinity prediction.

Let  $\mathbf{x}_{\text{mol}} \in \mathbb{R}^{d_m}$  denote the molecular feature vector obtained from Mordred descriptors, where  $d_m$  is the number of selected ligand descriptors. Similarly, let  $\mathbf{x}_{\text{prot}} \in \mathbb{R}^{d_p}$  denote the protein feature vector extracted from sequence and structural analysis, where  $d_p$  is the number of protein features. The final input vector is formed by concatenation:

$$\mathbf{x} = [\mathbf{x}_{\text{mol}} \parallel \mathbf{x}_{\text{prot}}] \in \mathbb{R}^{d_m+d_p}. \quad (1)$$

The FCNN consists of  $L$  hidden layers. For each hidden layer  $l \in \{1, 2, \dots, L\}$ , the transformation is defined as

$$\mathbf{h}^{(l)} = \sigma(\mathbf{W}^{(l)} \mathbf{h}^{(l-1)} + \mathbf{b}^{(l)}), \quad (2)$$

where  $\mathbf{h}^{(0)} = \mathbf{x}$ ,  $\mathbf{W}^{(l)} \in \mathbb{R}^{d_l \times d_{l-1}}$  and  $\mathbf{b}^{(l)} \in \mathbb{R}^{d_l}$  are the learnable weights and biases of the  $l$ -th layer, and  $\sigma(\cdot)$  is the non-linear activation function. In our implementation, the rectified linear unit (ReLU) was employed:

$$\sigma(z) = \max(0, z). \quad (3)$$

Dropout layers were applied between hidden layers to reduce overfitting, and batch normalization was used to stabilize training. The final prediction is produced by a linear projection from the last hidden representation

$$\hat{y} = \mathbf{W}^{(L+1)} \mathbf{h}^{(L)} + \mathbf{b}^{(L+1)}, \quad (4)$$

where  $\hat{y} \in \mathbb{R}$  corresponds to the predicted binding affinity

The ground-truth label  $y$  is the experimentally measured binding affinity, either in nanomolar (nM) scale or transformed into the logarithmic form

$$p\text{Affinity} = -\log_{10}(\text{Affinity in M}). \quad (5)$$

The network is trained to minimize the mean squared error (MSE) between the predicted affinities  $\hat{y}_i$  and the true values  $y_i$

$$\mathcal{L}_{\text{MSE}} = \frac{1}{N} \sum_{i=1}^N (y_i - \hat{y}_i)^2, \quad (6)$$

where  $N$  is the number of training samples. This loss encourages the model to produce predictions

close to the experimental affinities, while the pAf finity transformation provides a numerically stable scale for regression

## 4. Experiments

### 4.1. Implementation Details

All models were implemented in Python using PyTorch (version 2.0). Molecular descriptors were computed with Mordred, and protein features were extracted from UniProt sequences and AlphaFold-predicted structures. The input vectors were standardized with zero mean and unit variance before feeding into the network. The fully connected neural network consisted of three hidden layers with 512, 256, and 128 units, each followed by ReLU activation and dropout ( $p = 0.3$ ). Training was performed with the Adam optimizer ( $\beta_1 = 0.9$ ,  $\beta_2 = 0.999$ ) and an initial learning rate of  $1 \times 10^{-3}$ . The batch size was set to 64, and early stopping was applied with a patience of 20 epochs. Five-fold cross-validation was conducted on the training set, and the best model was evaluated on the independent test set.

### 4.2. Evaluation Metrics

To evaluate predictive performance, we used multiple regression and classification metrics. For regression, the following metrics were reported

$$\begin{aligned} \text{RMSE} &= \sqrt{\frac{1}{N} \sum_{i=1}^N (y_i - \hat{y}_i)^2}, \\ \text{MAE} &= \frac{1}{N} \sum_{i=1}^N |y_i - \hat{y}_i|, \\ r &= \frac{\sum_i (y_i - \bar{y})(\hat{y}_i - \bar{\hat{y}})}{\sqrt{\sum_i (y_i - \bar{y})^2} \sqrt{\sum_i (\hat{y}_i - \bar{\hat{y}})^2}}, \end{aligned} \quad (7)$$

where  $N$  is the number of samples,  $y_i$  is the ground-truth affinity, and  $\hat{y}_i$  is the predicted affinity. For classification-oriented evaluation, affinities were binarized at the threshold  $\text{pAffinity} > 7$  to indicate strong binders. We then reported AUC, precision, recall, and F1-score to assess model performance in distinguishing active vs. inactive compounds.

### 4.3. Experimental Results

We compared our FCNN framework with several baseline methods, including Random Forest (RF), Support Vector Regression (SVR), and Gradient Boosted Trees (XGBoost). As shown in Table 3, our method consistently outperformed the baselines across all metrics. In particular, the proposed FCNN achieved the lowest RMSE and MAE, and the highest Pearson correlation  $r$ , demonstrating superior regression accuracy. On the classification task, our method achieved an AUC of 0.92, compared to 0.84 (RF), 0.81 (SVR), and 0.86 (XGBoost). These results confirm that incorporating protein structural features alongside molecular descriptors provides a significant advantage in affinity prediction.

Table 3: Performance comparison between our FCNN framework and baseline models.  $\downarrow$  indicates lower is better;  $\uparrow$  indicates higher is better.

Method	RMSE $\downarrow$	MAE $\downarrow$	$r \uparrow$	AUC $\uparrow$
RF	1.32	1.04	0.71	0.84
SVR	1.45	1.12	0.67	0.81
XGBoost	1.28	0.98	0.74	0.86
FCNN (Ours)	1.05	0.82	0.81	0.92

### 4.4. Ablation Studies

To assess the contribution of different feature components, we conducted ablation experiments. Three model variants were evaluated: (1) ligand-only model using molecular descriptors (2) protein-

only model using transporter features, and (3) the full model with both ligand and protein features. Results are summarized in Table 4. The ligand-only model achieved moderate performance RMSE= 1.32 = 0.70], while the protein-only model performed slightly better (RMSE= 1.25,  $r = 0.73$ ). The full integrated model achieved the best performance (RMSE = 1.05 = 1.05 = 1.05 = 0.81), highlighting the complementary roles of ligand descriptors and protein structural features. This confirms that integrating both modalities is critical for accurate affinity prediction.

Table 4: Ablation study showing the effect of different feature sets.

Model Variant	RMSE ↓	MAE ↓	$r \uparrow$
Ligand-only	1.32	1.08	0.70
Protein-only	1.25	1.00	0.73
Full model (Ligand+Protein)	1.05	0.82	0.81

## 5. Discussion

The results of our study highlight several important findings. First, the integration of ligand-based descriptors with protein-derived features clearly improves prediction performance compared with traditional QSAR or ligand-only baselines. This indicates that protein structural information, even when derived from computational predictions such as AlphaFold, provides complementary signals that are critical for accurately modeling ligand transporter interactions. Second, the consistent improvements observed across multiple transporters suggest that our framework is not limited to a specific target, but can generalize to a broader range of neurotransmitter transporters associated with mood regulation. This generalizability is essential for practical drug discovery pipelines where new targets are frequently investigated.

Nevertheless, some limitations should be noted. The affinity data collected from public resources may contain inconsistencies due to different assay protocols, which introduces noise into the training process. In addition, our FCNN architecture captures global feature interactions but does not explicitly model spatial contacts between ligand atoms and protein residues. More advanced architectures, such as graph neural networks or attention-based models, could better capture fine-grained molecular interactions. Furthermore, the current framework focuses solely on static features, while dynamic aspects of protein-ligand interactions (e.g., conformational changes observed in molecular dynamics simulations) remain unmodeled. Addressing these limitations will be important for future work.

## 6. Conclusion

In this paper, we presented a fully connected neural network framework that integrates molecular descriptors and protein structural features for predicting ligand-transporter binding affinity. Our approach outperforms baseline methods and demonstrates the value of combining ligand and protein modalities. This framework offers a scalable and effective computational tool for screening candidate anxiolytic drugs, with the potential to accelerate discovery and reduce reliance on costly trial-and-error methods. In future work, we aim to extend this approach to more diverse protein families and explore hybrid models that incorporate sequence, structure and dynamics for improved affinity prediction.

## References

- [1] World Health Organization, “World mental health report: Transforming mental health for all” World Health Organization, 2023. [Online]. Available: <https://www.who.int/publications/item/9789240049338>
- [2] G. E. Torres, R. R. Gainetdinov, and M. G. Caron, “Neurotransmitter transporters: structure, function, and regulation,” *Nature Reviews Neuroscience*, vol. 4, no. 1, pp. 13–25, 2003.

[3] M. J. Owens and C. B. Nemeroff, "Neurotransmitter transporters and psychopharmacology," *Journal of Clinical Psychopharmacology*, vol. 17, no. 5, pp. S2-S23, 1997.

[4] J. Jumper, R. Evans, A. Pritzel et al., "Highly accurate protein structure prediction with alphafold," *Nature*, vol. 596, no. 7873, pp. 583-589, 2021.

[5] The Nobel Foundation, The nobel prize in chemistry 2024, <https://www.nobelprize.org/prizes/chemistry/2024/press-release/>, 2024.

[6] A. Cherkasov, E. N. Muratov, D. Fourches et al., "Qsar modeling: where have you been? where are you going to?" *Journal of Medicinal Chemistry*, vol. 57, no. 12, pp. 4977-5010, 2024.

[7] J. Jimenez, M. Skalic, G. Martinez-Rosell, and G. De Fabritis, "Kdeep: Protein-ligand absolute binding affinity prediction via 3d-convolutional neural networks," *Journal of Chemical Information and Modeling*, vol. 58, no. 2, pp. 287-296, 2018.

[8] H. Moriwaki, Y.-S. Tian, N. Kawashita, and T. Takagi, "Mordred: a molecular descriptor calculator," *Journal of Cheminformatics*, vol. 10, no. 1, pp. 1-14, 2018.

[9] M. K. Gilson, T. Liu, M. Baitaluk, G. Nicola, L. Hwang, and J. Chong, "Bindingdb in 2015: A public database for medicinal chemistry, computational chemistry and systems pharmacology," *Nucleic Acids Research*, vol. 44, no. D1, pp. D1045-D1053, 2016 [Online]. Available: <https://academic.oup.com/nar/article/44/D1/D1045/2502601>

[10] B. Zdrazil et al., "The chembl database in 2023: a drug discovery platform spanning multiple bioactivity data types and time periods," *Nucleic Acids Research*, vol. 52, no. D1, pp. D1180-D1192, 2024. [Online]. Available <https://academic.oup.com/nar/article/52/D1/D1180/7337608>

[11] S. Kim, J. Chen, T. Cheng, A. Gindulyte, J. He, S. He et al., "Pubchem 2019 update: improved access to chemical data," *Nucleic Acids Research*, vol. 47, no. D1, pp. D1102-D1109, 2019. [Online]. Available: <https://academic.oup.com/nar/article/47/D1/D1102/5146201>

[12] J.J. Irwin, T. Sterling, M. M. Mysinger, E.S. Bolstad, and R.G. Coleman, "Zinc: A free tool to discover chemistry for biology," *Journal of Chemical Information and Modeling*, vol. 52, no. 7, pp. 1757-1768, 2012. [Online]. Available <https://pubs.acs.org/doi/10.1021/ci3001277>

[13] T. U. Consortium, "Uniprot: the universal protein knowledgebase in 2021" *Nucleic Acids Research*, vol. 49, no. D1, pp. D480-D489, 2021. [Online]. Available: <https://academic.oup.com/nar/article/49/D1/D480/6006196>

[14] G. Landrum and contributors, "Rdkit: Open-source cheminformatics software," <http://www.rdkit.org>, 2016, [Online; accessed YYYY-MM-DD].

[15] A. P. Bento, A. Hersey, E. Felix et al., "An open source chemical structure curation pipeline using rdkit," *Journal of Cheminformatics*, vol. 12, p. 51, 2020. [Online] Available: <https://jcheminf.biomedcentral.com/articles/10.1186/s13321-020-00456-1>

[16] Y.-C. Cheng and W. H. Prusoff, "Relationship between the inhibition constant ( $k_i$ ) and the concentration of inhibitor which causes 50 per cent inhibition ( $i_{50}$ ) of an enzymatic reaction," *Biochemical Pharmacology*, vol. 22, no. 23, pp. 3099-3108, 1973. [Online]. Available: <https://pubmed.ncbi.nlm.nih.gov/4202581/>

[17] H. Moriwaki, Y.-S. Tian, N. Kawashita, and T. Takagi, "Mordred: a molecular descriptor calculator," *Journal of Cheminformatics*, vol. 10, no. 1, p. 4, 2018. [Online]. Available: <https://jcheminf.biomedcentral.com/articles/10.1186/s13321-018-0258-y>

[18] W. Kabsch and C. Sander, "Dictionary of protein secondary structure: pattern recognition of hydrogen-bonded and geometrical features," *Biopolymers*, vol. 22, no. 12, pp. 2577-2637, 1983. [Online]. Available: <https://pubmed.ncbi.nlm.nih.gov/6667333>

[19] S. Mitternacht, "Freesasa: An open source c library for solvent accessible surface area calculations," *F1000Research*, vol. 5, p. 189, 2016. [Online]. Available: <https://pmc.ncbi.nlm.nih.gov/articles/PMC4776673/>